

Isocorrole-Loaded Polymer Nanoparticles for Photothermal Therapy under 980 nm Light Excitation

Maximilian R. J. Marek,[†] Trong-Nhan Pham,[†] Jianxin Wang, Qiuqi Cai, Glenn P. A. Yap, Emily S. Day,* and Joel Rosenthal*



Cite This: *ACS Omega* 2022, 7, 36653–36662



Read Online

ACCESS |



Metrics & More

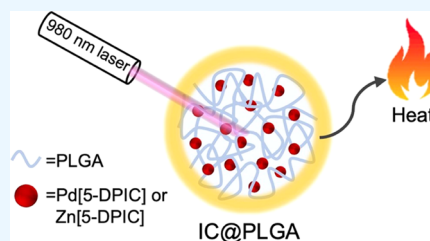


Article Recommendations



Supporting Information

ABSTRACT: Photothermal therapy (PTT) is a promising treatment option for diseases, including cancer, arthritis, and periodontitis. Typical photothermal agents (PTAs) absorb light in the near-infrared (NIR)-I region of 650–900 nm with a predominant focus around 800 nm, as these wavelengths are minimally absorbed by water and blood in the tissue. Recently, interest has grown in developing nanomaterials that offer more efficient photothermal conversion and that can be excited by light close to or within the NIR-II window of 1000–1700 nm, which offers less absorption by melanin. Herein, we report on the development of 5,5-diphenyl isocorrole (5-DPIC) complexes containing either Zn(II) or Pd(II) (Zn[5-DPIC] and Pd[5-DPIC], respectively) that absorb strongly across the 850–1000 nm window. We also show that poly(lactic-*co*-glycolic acid) (PLGA) nanoparticles loaded with these designer isocorroles exhibit low toxicity toward triple-negative breast cancer (TNBC) cells in the dark but enable efficient heat production and photothermal cell ablation upon excitation with 980 nm light. These materials represent an exciting new platform for 980 nm activated PTT and demonstrate the potential for designer isocorroles to serve as effective PTAs.



INTRODUCTION

Photothermal therapy (PTT) is an emerging treatment option for a variety of diseases, including cancer and arthritis, that involves localized irradiation of a photothermal agent (PTA).^{1–3} Upon irradiation, light energy is harnessed by the PTA and converted into thermal energy to yield localized hyperthermia. The induction of thermal stress can cause cells to undergo apoptosis at lower temperatures (ca. 42 °C) and necrosis at higher temperatures (ca. 49 °C), although the mechanism of cell death depends on numerous factors, including the length of time the temperature was maintained.² The ability to induce cell death with PTT has been successfully demonstrated in many cancer subtypes using varying wavelengths of light.^{3–5} One of the most important benefits of PTT is its minimally invasive nature, as only the targeted tumor area is irradiated, and systemic side effects are negligible.^{1,6}

When designing a PTA, the absorption wavelength is critical. While visible light (~400–700 nm) is readily absorbed by tissue components such as blood and water, longer wavelengths of light can penetrate tissue more deeply, thus allowing for the treatment of tumors in more difficult-to-reach locations.⁷ While most research has focused on making PTAs that absorb light in the near-infrared (NIR)-I region of 650–900 nm (*i.e.*, the conventional phototherapeutic window), recently, researchers have begun to explore the NIR-II region of 1000–1700 nm.⁸ Prior work has shown that nanoparticle contrast agents with NIR-II absorption can provide better imaging quality because there is less photon scattering in this

regime.^{7–9} NIR-II light also has better tissue tolerance, so PTAs that absorb in this spectral region may provide effective PTT with a greater safety window.^{10,11} Hence, more PTAs are being designed to have strong NIR-II absorption and efficient photothermal conversion. In this work, 980 nm light is used as the excitation wavelength for PTT. The advantage of 980 nm light is that it is less readily absorbed by melanin than 800 nm light (the most common wavelength used for PTT). Accordingly, while 800 nm light penetrates light-colored skin more deeply, 980 nm light penetrates more deeply into medium- and dark-colored skin, representing a potential benefit to large populations of patients.¹² A patient's skin pigmentation is an important consideration when selecting an excitation wavelength and corresponding PTA for PTT.

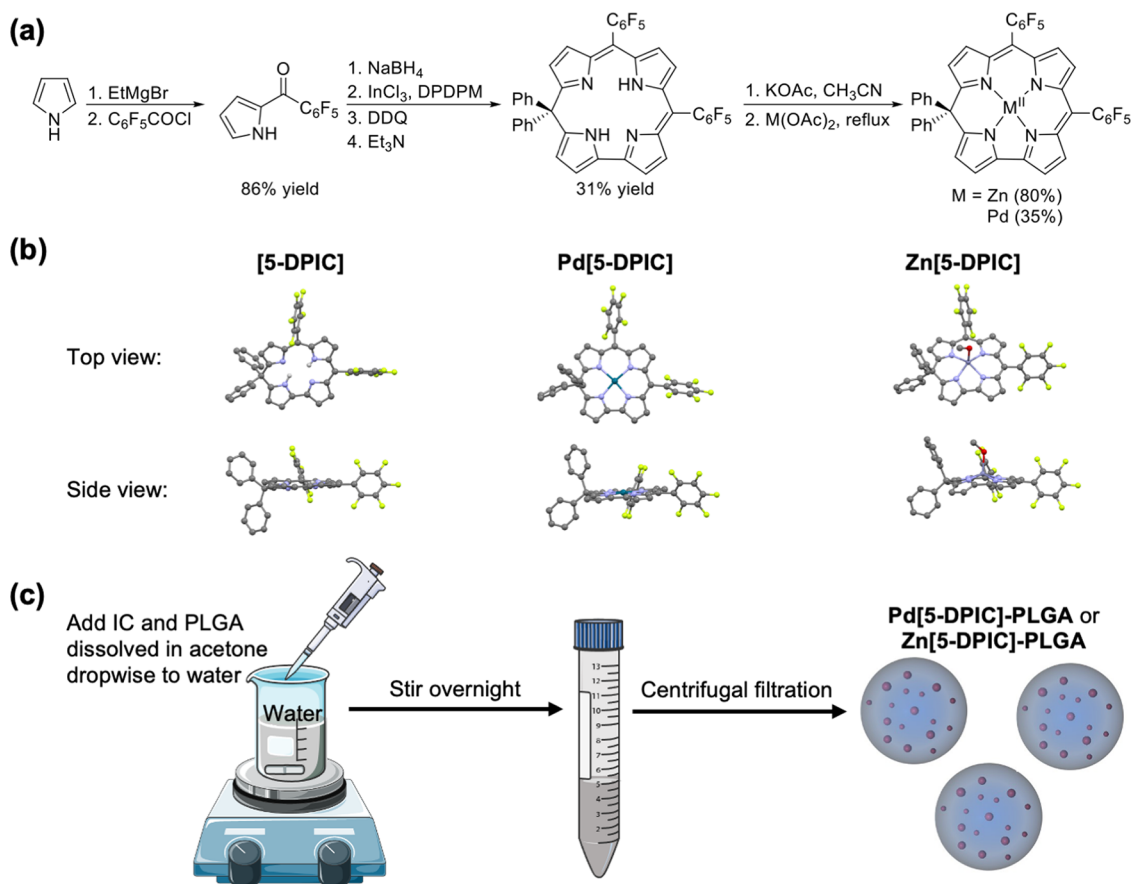
Herein, we introduce designer 5,5-diphenyl isocorrole ([5-DPIC]) complexes containing either Zn(II) or Pd(II) centers as potential agents for efficient PTT under 980 nm light excitation. The isocorrole is a π -conjugated tetrapyrrole macrocycle consisting of 19 atoms with *meso*-carbons that bridge pyrrole moieties at the 5-, 10-, and 15-positions.¹³ Unlike more traditional tetrapyrroles (*i.e.*, porphyrins, corroles,

Received: July 26, 2022

Accepted: September 22, 2022

Published: October 6, 2022



Scheme 1. Synthesis of 5-DPIC Derivatives and Encapsulation in PLGA-Based Nanoparticles^a

^a(a) Methodology employed for the chemical synthesis of 5-DPIC, Pd[5-DPIC], and Zn[5-DPIC]. (b) Solid state structures (from left to right) of [5-DPIC], Pd[5-DPIC], and Zn[5-DPIC] coordinated to one molecule of methanol, as viewed from the top (upper row) and from the side (lower row). All hydrogen atoms (except the pyrrolic protons of 5-DPIC) and disordered solvent molecules have been omitted for clarity. (c) Methodology employed to synthesize PLGA NPs loaded with either Pd[5-DPIC] or Zn[5-DPIC]. Portions of the schemes shown in this figure were generated using Servier Medical Art templates (<https://smart.servier.com>), which is licensed under a Creative Commons Attribution 3.0 Unported License.

phthalocyanines, etc.) that are aromatic in nature, isocorroles are nonaromatic owing to the presence of an sp^3 -hybridized *meso*-carbon bearing geminal alkyl or aryl substituents at either the 5- or 10-position. Accordingly, isocorroles are members of the growing family of nonaromatic tetrapyrrole frameworks that include phlorins and biladienes, and that support redox, photophysical, light harvesting, and catalytic properties that are unique from much more well-studied aromatic tetrapyrrole architectures.^{14–21}

Prior work has centered on the development of isocorroles bearing geminal dimethyl substituents at either the 5- or 10-positions.^{15,19} Stable dimethyl isocorroles complexed to divalent metal ions, including Co(II), Cu(II), Zn(II), and Pd(II),²² have been characterized, and both spectroscopic and computational²³ work have resolved the ability of such systems to absorb NIR light.^{21,22} Moreover, introduction of various different substituents onto the isocorrole backbone can expand the absorption band further into the NIR-II window.^{10,11}

Building on this precedent, we have prepared a set of metalloisocorroles bearing geminal diphenyl substituents at the macrocycles' sp^3 -hybridized 5-position. In addition to preparing the first freebase 5,5-diphenyl isocorrole derivative (5-DPIC), the Zn(II) and Pd(II) complexes were also prepared and characterized. Both Zn[5-DPIC] and Pd[5-DPIC] feature

intense absorbances spanning the NIR-I and NIR-II windows and can efficiently produce heat upon 980 nm light excitation. We show that these metalloisocorroles can be encapsulated in poly(lactic-*co*-glycolic acid) (PLGA) nanoparticles and evaluate their potential as PTAs *in vitro* using triple-negative breast cancer (TNBC) as a model disease, which is an aggressive breast cancer subtype that afflicts approximately 15–20% of breast cancer patients.^{24,25} TNBC does not express the progesterone receptor, estrogen receptor, and human epidermal growth factor-2 (HER-2) receptor, which makes it unsusceptible to hormone therapy and other forms of targeted chemotherapy such as trastuzumab.²⁵ Since TNBC can only be treated with nonselective forms of chemotherapy, radiation, and surgical methods, patients face debilitating secondary side effects such as hair loss, nausea, and lymphedema.^{26–28} Accordingly, PTT may be a particularly useful treatment for TNBC because it can provide localized, effective therapy independent of tumor biology. Indeed, PTT mediated by both NIR-I^{29,30} and NIR-II³¹ nanomaterials has shown promise against TNBC.

Our studies as disclosed herein show that Zn(II) and Pd(II) isocorroles encapsulated in PLGA nanoparticles are nontoxic to TNBC cells in the dark and serve as effective PTAs upon 980 nm light excitation. These findings warrant the continued

development of isocorroles with NIR-I and NIR-II absorption for effective PTT of different diseases.

METHODS

X-ray Structural Analysis of Isocorrole Derivatives.

Isocorroles were prepared according to methods detailed in the Supporting Information (SI) and illustrated in Scheme 1a. The synthesized isocorroles include 5,5-diphenyl-10,15-bis-(pentafluorophenyl)isocorrole (**5-DPIC**), as well as the Pd(II) and Zn(II) complexes of this isocorrole macrocycle (**Pd[5-DPIC]** and **Zn[5-DPIC]**, respectively). The structure of each (Scheme 1b) was determined by single-crystal X-ray diffraction. Crystals were mounted using viscous oil onto a plastic mesh and cooled to the data collection temperatures. Data were collected on a Bruker-AXS APEX II DUO CCD diffractometer with graphite monochromated Mo $K\alpha$ radiation ($\lambda = 0.71073 \text{ \AA}$) for **Pd[5-DPIC]** and **Zn[5-DPIC]**, and with Cu $K\alpha$ radiation ($\lambda = 1.54178 \text{ \AA}$) focused with Goebel mirrors for the freebase isocorrole (**5-DPIC**). Unit cell parameters were obtained from 36–48 data frames ($0.5^\circ \omega$) from different sections of the Ewald sphere.³² The systematic absences in the diffraction data were consistent uniquely for $P21/n$ for **5-DPIC** and **Pd[5-DPIC]**, and with Pc and $P2/c$ for **Zn[5-DPIC]**. The occupancy of 2 and the absence of either a molecular inversion center or a 2-fold rotation axis in **Zn[5-DPIC]** is consistent with the noncentrosymmetric space group option Pc , which yielded chemically reasonable and computationally stable results of refinement. Refinement of the absolute structure parameter yielded nil within experimental error, indicating the true hand of the data has been established. The data were treated with multiscan absorption corrections.³² The structures were solved using intrinsic phasing methods³³ and refined with full-matrix, least-squares procedures on F^2 .³⁴

A methanol solvent molecule was located coordinated to the Zn(II) center in **Zn[5-DPIC]**, with a second methanol molecule found within H-bonding distance to the coordinated solvent. The penultimate difference maps for **Pd[5-DPIC]** and **Zn[5-DPIC]** showed diffused electron densities that could not be modeled as identifiable solvent molecules. These were treated with Squeeze³⁵ and ignored in the empirical formula. All non-H atoms were refined with anisotropic displacement parameters. H atoms were constrained in idealized positions with isotropic parameters based on their attached atoms. Atomic scattering factors are contained in the SHELXTL program library.³⁴ The three structures have been deposited at the Cambridge Structural Database under deposition numbers CCDC 2206813 (**5-DPIC**), 2206814 (**Pd[5-DPIC]**), and 2206815 (**Zn[5-DPIC]**).

Isocorrole Encapsulation in PLGA Nanoparticles and Physicochemical Characterization. **Pd[5-DPIC]** and **Zn[5-DPIC]** were encapsulated in PLGA nanoparticles (NPs), as shown in Scheme 1c. Metalated isocorroles were dissolved in acetone at 5 mg/mL and stored as solutions at -20°C until use. To prepare isocorrole-loaded NPs (IC-NPs), 50:50 PLGA (39.5 kDa, 0.67 dL/g) was dissolved at 1 mg/mL in acetone while stirring, then $5.64 \times 10^6 \mu\text{M}$ **Pd[5-DPIC]** or $5.91 \times 10^6 \mu\text{M}$ **Zn[5-DPIC]** in acetone was added (157.3 μL per 1 mL PLGA-acetone or 150 μL per 1 mL of PLGA-acetone, respectively). Next, 2.0 mL of the isocorrole-PLGA solution was added to 6.0 mL of water in a 20 mL glass scintillation vial and stirred overnight at 800 rpm uncapped to allow for evaporation of acetone from the aqueous mixture. Afterward, NPs were collected and twice filtered through a 10

kDa centrifugal tube at 4200 rpm for 15 min. A third wash step was also completed over the course of 20 min. The filtrate was discarded, and 3.0 mL of fresh water was added after each centrifugation step. If necessary, nonencapsulated material was removed by centrifugation in 1.5 mL centrifuge tubes for 5 min at 750 rpm, with the supernatant removed and discarded.

Following synthesis, the hydrodynamic diameter and ζ -potential of the IC-loaded PLGA NPs were determined using an Anton Paar LiteSizer500 dynamic light scattering (DLS) instrument. Additionally, the samples were visualized using transmission electron microscopy (TEM) to reveal their morphology. TEM was performed using a Zeiss Libra 120 transmission electron microscope, as has previously been described.³⁶

UV–Vis Spectrophotometry of Free and Encapsulated Isocorroles. Ultraviolet–visible (UV–vis) absorption spectra of free **5-DPIC**, **Pd[5-DPIC]**, and **Zn[5-DPIC]** were collected at room temperature on a StellarNet CCD array UV–vis spectrometer using quartz cuvettes (6Q) with a 1.0 cm path length from Starna Cells, Inc. Spectra were collected in acetone containing each of the isocorrole derivatives at concentrations of 5.0, 10.0, 15.0, 20.0, and 25.0 μM .

Isocorrole-loaded NPs (IC-NPs) were diluted 1:50 with water before being analyzed by UV–vis spectroscopy using a Cary 60 spectrophotometer. A baseline of water was recorded, and the absorption spectrum was measured between 400–1100 nm to reveal the concentration of the encapsulated isocorroles. Once the concentration was determined, a stock solution of the IC-NPs was prepared in water with an optical density (OD) of 10 at 980 nm (the wavelength of the laser used in photothermal experiments). This stock solution was diluted for further experiments as necessary to yield samples with $\text{OD}_{980\text{nm}} = 5.0, 2.5, \text{ or } 1.0$.

Characterization of IC-PLGA NP Heating under 980 nm Light Excitation. For heating characterization studies, 450 μL of water was mixed with 50 μL of stock IC-NPs at $\text{OD}_{980\text{nm}} = 10, 5, 2.5, \text{ or } 1$ to yield samples with final $\text{OD}_{980\text{nm}}$ of 1.0, 0.5, 0.25, or 0.1. These solutions were placed in a polycarbonate cuvette (path length = 1.0 cm) with a magnetic stir bar and heated on a stir plate set at 320 rpm and 40°C for at least 2 h prior to irradiation to bring the solution temperature close to body temperature. The IC-NP samples were then exposed to 980 nm light using a LiteForce FXi (LiteCure) continuous wave laser at 0.5 W/cm^2 for 10 min. Thermal images were captured using a FLIR-6EX series camera every 30 s during irradiation. The experiment was repeated three times using separate batches of IC-NPs to characterize the materials' heating ability.

To examine the cyclic heating properties of the IC-loaded NPs, samples were irradiated with the 980 nm LiteForce FXi laser at 0.1 W/cm^2 for 5 min and allowed to cool for 10 min before repeating the irradiation and cooling cycle two additional times. Thermal images were captured using the FLIR-6EX series camera every 30 s during irradiation and every 60 s without irradiation.

In Vitro Evaluation of PTT Mediated by IC-NPs. MDA-MB-231 cells were thawed from a cryovial and cultured in Dulbecco's modified Eagle's medium (DMEM) supplemented with 10% fetal bovine serum (FBS) and 1% penicillin-streptomycin in tissue culture flasks (T-75) until reaching 80–90% confluency, at which point they were seeded at a density of 1×10^5 cells/well in a 96-well plate. After allowing the cells to adhere overnight, 90 μL of fresh media was added

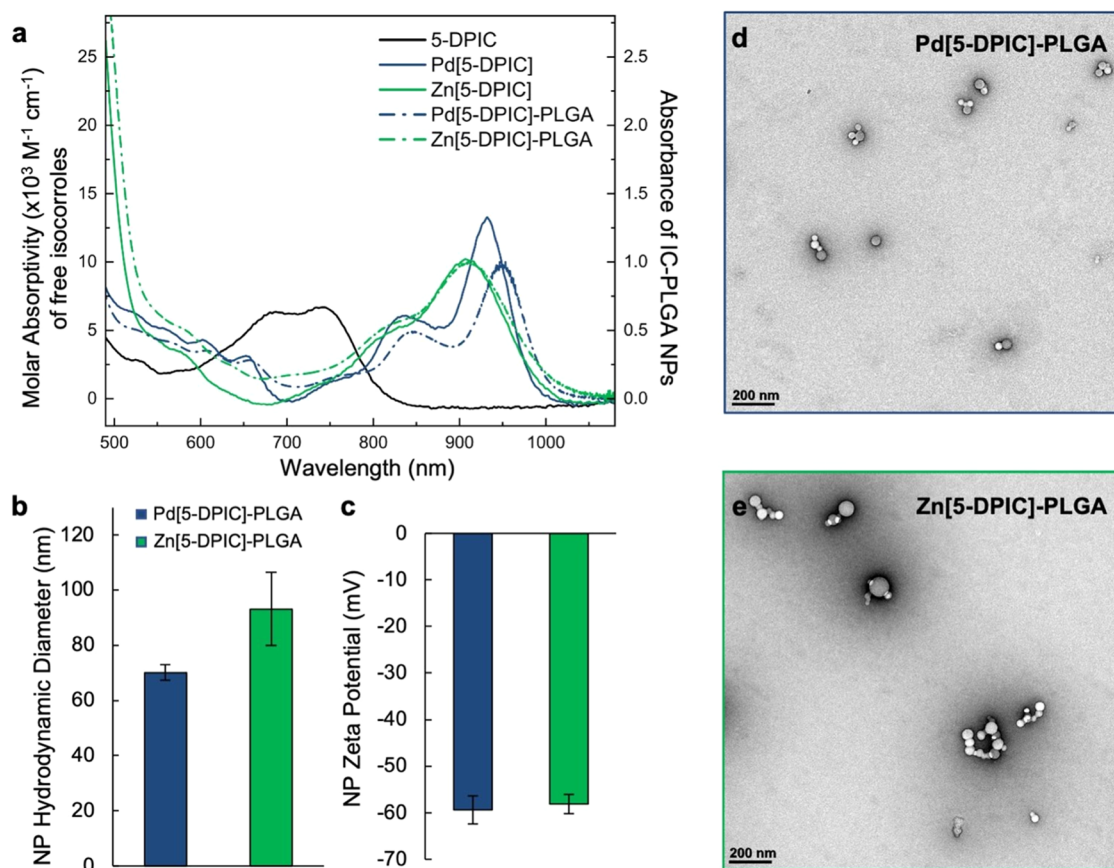


Figure 1. Characterization of IC-PLGA NPs. (a) Absorption profiles of 5-DPIC (solid black), Pd[5-DPIC] (solid blue), and Zn[5-DPIC] (solid green), along with absorption spectra of Pd[5-DPIC]-PLGA (dashed blue) and Zn[5-DPIC]-PLGA (dashed green) normalized to NIR λ_{\max} . (b) Hydrodynamic diameter of Pd[5-DPIC]-PLGA (blue) and Zn[5-DPIC]-PLGA (green) ($n = 3$; error bars represent standard deviation). (c) ζ -potential of Pd[5-DPIC]-PLGA (blue) and Zn[5-DPIC]-PLGA (green) ($n = 3$; error bars represent standard deviation). (d, e) Transmission electron microscopy images of Pd[5-DPIC]-PLGA (d) and Zn[5-DPIC]-PLGA (e).

to each well along with 10 μL of NPs at a stock concentration of $\text{OD}_{980\text{nm}} = 10, 5, 2.5,$ or 1 such that the final $\text{OD}_{980\text{nm}}$ in the wells was $1.0, 0.5, 0.25,$ or 0.1 . After incubating at 37°C for 6 h with the IC-loaded NPs, samples were irradiated for 8 min/well at $0.5\text{ W}/\text{cm}^2$ or were left unirradiated for a negative control. After 24 h, the media in each well was replaced with a mixture of 10 μL Alamar Blue and 90 μL DMEM to allow for measurement of cellular metabolic activity. After incubating at 37°C for 3 h, the Alamar Blue fluorescence was read at 560 nm excitation/590 nm emission with a Synergy H1M plate reader.

Statistical Analysis. Each experiment was performed in triplicate. Results are presented as mean \pm standard deviation. Statistical analysis was performed using one-way ANOVA with post hoc Tukey to determine the significance at the 95% confidence level.

RESULTS AND DISCUSSION

Synthesis and Characterization of 5,5-Diphenyl Isocorrole Derivatives. The synthesis of the 5,5-diphenyl-10,15-bis(pentafluorophenyl)isocorrole (5-DPIC) presented in Scheme 1a began with the preparation of 2-pentafluorobenzoyl pyrrole *via* condensation of pyrrole with pentafluorobenzoyl chloride (see the Supporting Information for full preparatory procedures). Reduction of this ketone with NaBH_4 , followed by addition of 5,5-diphenyldipyrromethane provided the freebase 5-DPIC in 31% yield following

purification by chromatography on silica (see the Supporting Information). The precursors pentafluorobenzoyl pyrrole and 5,5-diphenylpyrrole were synthesized *via* adaptation of previously described methods.^{37,38} This two-step synthesis provides a more streamlined and expedient route to the 5-DPIC tetrapyrrole over previous three-step routes to 5-dimethyl-substituted isocorroles.^{39,40}

Metalation of the freebase isocorrole was accomplished *via* treatment with KOAc in MeCN to deprotonate the pyrrole protons, followed by addition of 3 equiv of either $\text{Pd}(\text{OAc})_2$ or $\text{Zn}(\text{OAc})_2$ to deliver the corresponding Pd(II) (Pd[5-DPIC]) or Zn(II) (Zn[5-DPIC]) isocorrole complexes. The molecular structures of 5-DPIC, Pd[5-DPIC], and Zn[5-DPIC] were each confirmed by single-crystal X-ray diffraction studies. The molecular structures of these three isocorrole derivatives are reproduced in Scheme 1b and clearly demonstrate the planar geometry of the 5,5-diphenyl isocorrole scaffold, both with and without divalent metal centers coordinated within the tetrapyrrole cavity.

Isocorroles Maintain Their Absorption Spectrum following Encapsulation in PLGA NPs. The UV–vis absorption spectra of unencapsulated Pd[5-DPIC] and Zn[5-DPIC] were recorded in acetone and are shown in Figure 1a. The absorption spectrum for both of these isocorrole complexes and the freebase 5-DPIC derivative across the entire visible/NIR regions is also provided in Figure S1. Much like the freebase 5-DPIC (Table 1 and Figures 1 and

Table 1. Photophysical Properties of Isocorrole-Based Light Absorbers^a

isocorrole-based absorber	λ_{abs} (nm)	$\epsilon \times 10^3$ ($\text{M}^{-1} \text{cm}^{-1}$)
5-DPIC ^a	339	30.6 ± 2.8
	419	32.5 ± 3.0
	687	6.7 ± 0.3
	744	6.9 ± 0.2
Pd[5-DPIC] ^a	368.5	25.1 ± 3.1
	448	35.3 ± 1.3
	835	5.6 ± 0.5
	932	12.0 ± 1.2
Zn[5-DPIC] ^a	357	26.0 ± 1.3
	463	42.8 ± 3.6
	810	sh
Pd[5-DPIC]-PLGA ^b	906.5	10.1 ± 0.1
	450	N/A ^c
	848	
Zn[5-DPIC]-PLGA ^b	953	
	460	N/A ^d
	810	
	910	

^aSpectroscopic data of 5-DPIC, Pd[5-DPIC], and Zn[5-DPIC] are collected in acetone. ^bSpectroscopic data of Pd[5-DPIC]-PLGA and Zn[5-DPIC]-PLGA are collected in water. ^cAbsorption at 953 nm are normalized to 1.0. ^dAbsorption at 910 nm are normalized to 1.0. ^esh = shoulder.

S1), both the Zn(II) and Pd(II) isocorrole complexes strongly absorb light between 350 and 500 nm, which corresponds to the intense Soret-type band typical of porphyrinic chromophores.⁴¹ The introduction of Zn(II) and Pd(II) centers into the 5-DPIC scaffold gives rise to an increase in maximum extinction coefficients in the Soret region (from $\epsilon_{\text{max}} \sim 32,500 \text{ M}^{-1} \text{cm}^{-1}$ for freebase 5-DPIC to $\epsilon_{\text{max}} \sim 35,300$ and $42,800 \text{ M}^{-1} \text{cm}^{-1}$ for Pd[5-DPIC] and Zn[5-DPIC], respectively).

Of greater import for PTT applications, both Pd[5-DPIC] and Zn[5-DPIC] support relatively intense absorption features across the NIR-I and into the NIR-II spectral regions. These significant long energy absorption bands from ~ 800 – 1000 nm are red-shifted by approximately 200 nm relative to the longest wavelength features observed for the freebase congener (*i.e.*, ~ 650 – 785 nm, see Figure S1). The extinction coefficients of the NIR absorption features for Pd[5-DPIC] and Zn[5-DPIC] ($\epsilon \sim 12,000$ and $10,100 \text{ M}^{-1} \text{cm}^{-1}$, respectively) are both larger than the extinction coefficient of the most red-shifted features observed for the freebase 5-DPIC ($\epsilon \sim 6,900 \text{ M}^{-1} \text{cm}^{-1}$ at 744 nm). While the NIR absorption features of both metalloisocorroles tail off at ~ 1000 nm, both compounds are strong absorbers in the NIR with overlap into the NIR-II region. Based on the above, we found the Pd[5-DPIC] and Zn[5-DPIC] frameworks to be well positioned for testing as potential phototherapeutic agents of interest. Notably, the ability of Pd[5-DPIC] and Zn[5-DPIC] to absorb NIR-II light is vastly improved relative to that of other Zn(II), Co(II), Cu(II), Ni(II), and Pd(II) isocorrole complexes that do not bear geminal diphenyl substituents at the sp^3 -hybridized meso-carbon.^{15,19,21,42} Indeed, Zn(II) isocorrole homologues bearing geminal methyl groups at the sp^3 -hybridized 5-position support a NIR λ_{max} at ~ 850 nm (as opposed to 905 nm for Zn[5-DPIC]) and do not absorb at wavelengths longer than ~ 920 nm.²¹ Accordingly, the installation of geminal diphenyl substituents at the 5-position of the isocorrole appears

important to enhancing the ability of these platforms to strongly absorb light at wavelengths longer than ~ 950 nm.

Despite the attractive light-absorbing properties of Pd[5-DPIC] and Zn[5-DPIC], both are not directly applicable for use as phototheranostic agents since like most tetrapyrrole constructs, isocorroles are hydrophobic and insoluble in aqueous media. As a means to water-solubilize the metalloisocorroles and improve their biocompatibility, we prepared PLGA nanoparticles encapsulating either Pd[5-DPIC] and Zn[5-DPIC] using well-established single emulsion protocols,³⁶ as illustrated in Scheme 1c. Freshly prepared isocorroles that were stored at -20 °C away from light were initially dissolved at 10 mg/mL in acetone and added to PLGA dissolved in acetone at a concentration of 1 mg/mL. This mixture was added dropwise to 6 mL of water and allowed to stir overnight to evaporate out any acetone. The nanoparticles were then collected in a 50 kDa filter centrifuge tube and centrifuged three times with the water in the bottom of the centrifuge tube discarded and 3 mL of water added to the top portion as a wash step. After centrifugal filtration, nanoparticles were collected and stored away from visible light as a precaution to prevent degradation of the isocorroles prior to further characterization studies. We note that prior work has demonstrated that freebase 5,5-dimethylisocorrole is stable under illumination for at least 2 weeks.⁴⁰

The absorption profiles recorded for samples of Pd[5-DPIC]-PLGA and Zn[5-DPIC]-PLGA in water show nearly identical features with slight bathochromic shifts (peak $\lambda_{\text{abs}} \sim 953$ and 910 nm, respectively) relative to those observed for the free metalloisocorroles in acetone (see Figures 1a and S1, and Table 1). These results indicate that Pd[5-DPIC] and Zn[5-DPIC] are stable when loaded within PLGA NPs, and their prominent NIR absorption features are retained, if not slightly enhanced, upon encapsulation. Based on the above, we set out to characterize and evaluate the physicochemical properties and photothermal activity of both sets of IC-loaded PLGA NPs upon activation with light from the high-energy end of the NIR-II spectral region.

Physicochemical Properties of Pd[5-DPIC]-PLGA and Zn[5-DPIC]-PLGA. PLGA NPs loaded with Pd[5-DPIC] or Zn[5-DPIC] were characterized by DLS, ζ -potential measurements, and TEM. The hydrodynamic diameters of the Pd[5-DPIC]-PLGA and Zn[5-DPIC]-PLGA NPs were determined to be 73.1 ± 2.8 and 93 ± 13.2 nm, respectively (see Figure 1b). This size regime is ideal for therapeutic application, as NPs with a diameter below 200 nm demonstrate maximal accumulation in tumors, which has long been attributed to the enhanced permeability and retention (EPR) effect but may also result from endothelial transcytosis.^{43,44} In addition, both NP types displayed a negative ζ -potential (Figure 1c), which is important since negatively charged NPs generally exhibit longer circulation time than positive NPs due to reduced protein absorption.⁴⁵ The NPs were also visualized by TEM, which showed they are spherical and relatively monodisperse in size and morphology (Figure 1d,e).

Isocorrole-Loaded PLGA NPs are Efficient Photothermal Converters under 980 nm Excitation. Having found that the NIR light absorption and physicochemical properties of the Pd[5-DPIC]-PLGA and Zn[5-DPIC]-PLGA NPs were potentially well suited for phototherapeutic applications, we worked to evaluate the photothermal activity of these systems using an excitation source toward the high-energy end of the NIR-II region. Samples of Pd[5-DPIC]-

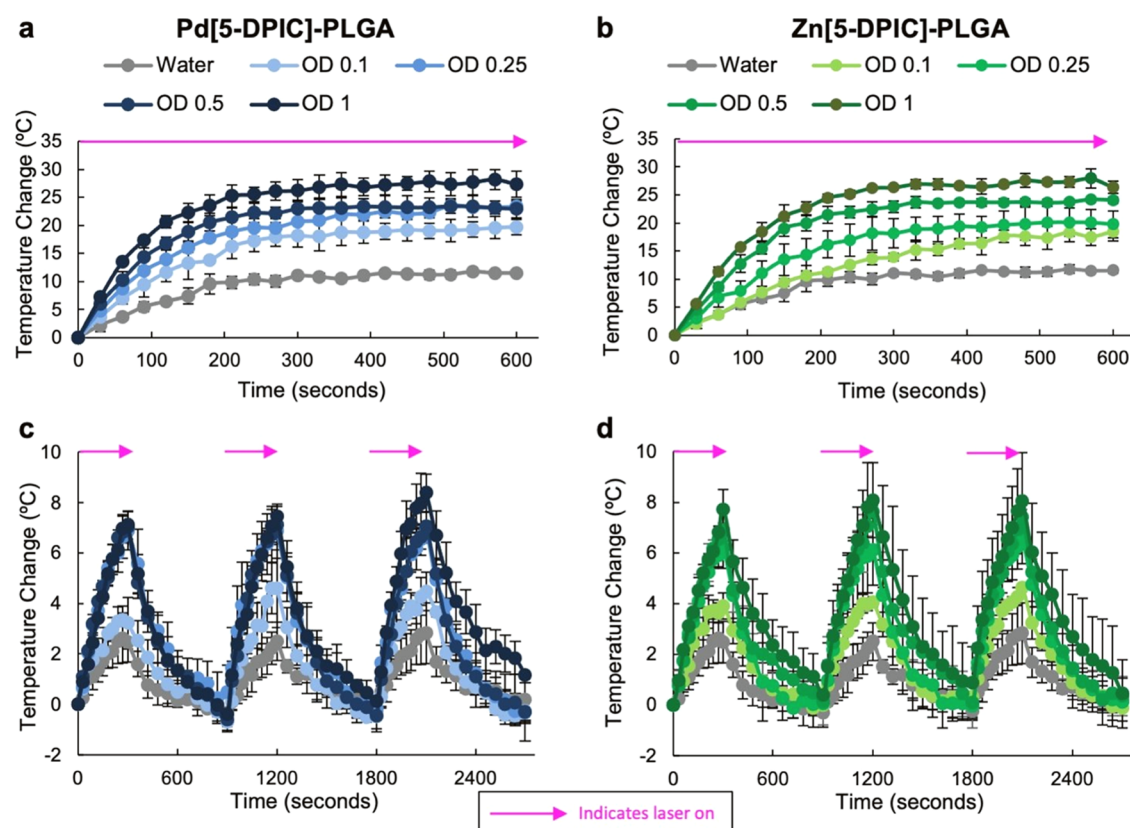


Figure 2. Heating characterization of Pd[5-DPIC]-PLGA and Zn[5-DPIC]-PLGA. Heating profile of (a) Pd[5-DPIC]-PLGA and (b) Zn[5-DPIC]-PLGA at various loadings in water upon irradiation at 980 nm for 10 min at 0.5 W/cm². Cyclic heating of (c) Pd[5-DPIC]-PLGA and (d) Zn[5-DPIC]-PLGA in water, where samples were irradiated at 980 nm for 5 min at 0.1 W/cm² and cooled for 10 min, repeated thrice. All results are from $n = 3$ trials, and error bars indicate standard deviation.

PLGA and Zn[5-DPIC]-PLGA were irradiated with 980 nm light of 0.5 W/cm² intensity over a 10 min period to characterize NP heating capacity and assess (1) the rate of temperature increase, (2) the length of time required for NPs to achieve maximum solution temperature, and (3) the relationship between NP concentration and maximum temperature realized. As shown in Figure 2a,b, both the Pd[5-DPIC]-PLGA and Zn[5-DPIC]-PLGA NPs demonstrated an increased heating response compared to a water control. Both of the encapsulated isocorrole samples also showed an increase in temperature change from baseline with increasing OD over the course of irradiation. Notably, the Pd[5-DPIC]-PLGA NPs demonstrated a greater increase in temperature across each of the different concentrations compared to the Zn[5-DPIC]-PLGA NPs, particularly during the first 2 min of irradiation. This improved heating response is likely due to the peak NIR absorption of the Pd[5-DPIC] being closer to the 980 nm laser excitation wavelength than the peak absorption of the Zn[5-DPIC]. Both types of NP exhibited the greatest rate of temperature increase over the first 5 min of irradiation, after which the solution temperature plateaued.

To understand whether IC-PLGA NPs maintain their heating ability post-irradiation, cyclic heating studies were performed, wherein the NPs were irradiated with 980 nm light of 0.1 W/cm² intensity for 5 min, followed by a 10 min cooling period with the laser off. Temperature cycling was repeated three times. As with the extended heating studies (*vide supra*), cyclic heating trials showed that IC-PLGA NPs reached higher temperatures upon irradiation than a water control group

(Figure 2c,d). At 0.1 OD, both the Pd[5-DPIC]-PLGA and Zn[5-DPIC]-PLGA NPs achieved a temperature rise of ~4 °C from baseline during each irradiation cycle. At higher ODs, the maximum temperature attained was ~7–8 °C above baseline for each of the irradiation cycles. The excellent repeatability of the photothermal heating–cooling cycles demonstrates that the NPs and the encapsulated ICs can reach therapeutically relevant temperatures upon cyclic irradiation at 980 nm at the laser powers highlighted above. Notably, the Pd[5-DPIC]-PLGA NPs did exhibit a heightened ability to convert light to thermal energy, suggested by the more complete dissipation of the heat converted from light during the 10 min cooling cycle over the Zn(II) congeners (*vide infra*). This could also be due to the Pd[5-DPIC] complex's peak NIR absorption (~958 nm) being closer to that of the laser source than that for Zn[5-DPIC] (~910 nm).

Following the methodology and analysis demonstrated by Roper and co-workers,⁴⁶ the photothermal conversion efficiency (PCE) of the IC-loaded NPs was calculated from the heating and cooling data shown in Figure 2, as described in the Supporting Information. The PCE of Zn[5-DPIC]-PLGA was 18.5% under 0.1 W/cm² irradiation at 980 nm, compared to 58.6% for Pd[5-DPIC]-PLGA. These values are comparable to the ~23% PCE under 980 nm light excitation determined for gold nanorods, one of the most studied PTAs, and the ~31% PCE found for black phosphorous nanosheets in the same study.⁴⁷ The PCEs determined for the encapsulated isocorroles are also comparable to the ~19.2% PCE of graphitic carbon nanocages and the ~21.1% PCE of multi-

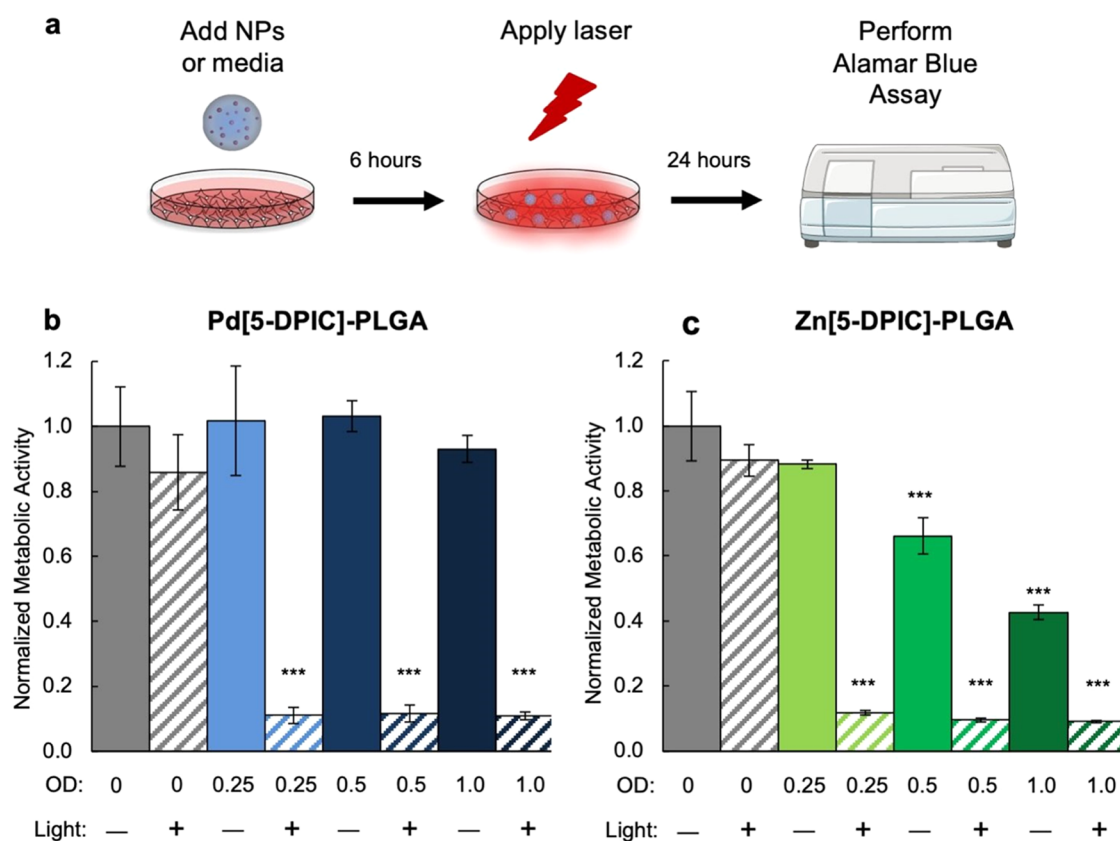


Figure 3. Metabolic activity of MDA-MB-231 cells exposed to IC-PLGA NPs in the absence or presence of 980 nm light. (a) Experimental design showing cells were treated with NPs for 6 h prior to irradiation and subsequent analysis of metabolic activity *via* Alamar Blue assay. (b) Metabolic activity of MDA-MB-231 cells treated with Pd[5-DPIC]-PLGA NPs with and without irradiation. (c) Metabolic activity of MDA-MB-231 cells treated with Zn[5-DPIC]-PLGA NPs with and without irradiation. *** indicates $p < 0.001$ vs untreated control ($OD_{980\text{nm}} = 0$, no light) by one-way ANOVA with post hoc Tukey.

walled carbon nanotubes found in recent work.⁴⁸ While the PCE of the IC-loaded NPs is below the record of $\sim 79\%$ found for spiky gold nanoparticles under 980 nm light excitation,⁴⁹ the Zn[5-DPIC]-PLGA and Pd[5-DPIC]-PLGA NPs have sufficient PCE to induce tumor heating above damage thresholds and offer the benefit of utilizing materials that readily degrade in the body, whereas gold will bioaccumulate.

IC-PLGA NPs Exhibit Low Dark Toxicity and Provide Efficient PTT of TNBC Cells upon 980 nm Irradiation. To evaluate the cytocompatibility and photothermal efficacy of the IC-PLGA NPs, MDA-MB-231 TNBC cells were treated with varying concentrations of the NPs and were either left unirradiated or exposed to 980 nm light for 8 min at 0.5 W/cm^2 . Following treatment, the cellular metabolic activity of the TNBC cells was assessed by Alamar Blue assay, as depicted in Figure 3a. Upon irradiation, both Pd[5-DPIC]-PLGA and Zn[5-DPIC]-PLGA significantly decreased MDA-MB-231 metabolic activity by $\sim 90\%$ across all tested concentrations, indicating both NP types are efficient PTAs (Figure 3b,c). The difference in viability between untreated and NP-treated cells in the presence of light was statistically significant ($p < 0.01$) when analyzed by one-way ANOVA with post hoc Tukey. The lack of statistical difference in viability between NP-treated cells across different concentrations is likely due to the high efficacy even at low OD. That is, once enough NPs have been added to the samples such that they cross a specific temperature/damage threshold upon irradiation, further increasing the OD to produce more heat has little additional

effect on the cells that can be identified within the sensitivity of the assay. In the absence of irradiation, cells exposed to Pd[5-DPIC]-PLGA maintained metabolic activity above 90%, indicating a lack of dark toxicity at concentrations ranging from $OD_{980\text{nm}} = 0.1$ – 1.0 (Figure 3b). The negligible dark toxicity of Pd[5-DPIC]-PLGA coupled with its excellent potency upon irradiation indicates the encapsulated Pd(II) isocorrole complex is an ideal mediator of PTT since it offers a high therapeutic ratio/safety window.^{3,5,6,50}

We found that Zn[5-DPIC]-PLGA was nontoxic to cells in the dark at concentrations up to $OD_{980\text{nm}} = 0.25$, but cellular metabolic activity decreased substantially when cells were exposed to Zn[5-DPIC]-PLGA at $OD_{980\text{nm}} = 0.5$ or 1.0 (Figure 3c). Specifically, cell metabolic activity was 66% following exposure to Zn[5-DPIC]-PLGA at $OD_{980\text{nm}} = 0.5$ and 43% when treated at $OD_{980\text{nm}} = 1.0$. This decreased metabolic activity in the absence of light agrees with prior work that has shown zinc-based NPs can have cytotoxic effects.^{51,52} One possible reason for the observed dark toxicity of the Zn[5-DPIC]-PLGA at concentrations $OD_{980\text{nm}} = 0.5$ or 1.0 could be leaching of the Zn[5-DPIC] tetrapyrrole complex or free Zn(II) ions out of the PLGA NPs since this isocorrole is more prone to demetallation than the Pd[5-DPIC] congener. Since Zn(II) ions can be naturally cytotoxic,⁵² this direct exposure at higher concentrations may explain the dark toxicity observed upon treatment with Zn[5-DPIC]-PLGA at higher concentrations. Nevertheless, the data show that Zn[5-DPIC]-PLGA NPs can be utilized safely for PTT at concentrations below

$OD_{980nm} = 0.25$, where there is low dark toxicity coupled with highly efficient photo-triggered cell death using 980 nm light. However, given that Zn[5-DPIC]-PLGA has a lower therapeutic ratio/safety window than Pd[5-DPIC]-PLGA, the latter is more suitable for future development toward *in vivo* application.

CONCLUSIONS AND FUTURE DIRECTIONS

This study demonstrates the successful synthesis of the designer isocorroles Pd[5-DPIC] and Zn[5-DPIC] and shows they can be encapsulated in NPs and exploited as novel PTAs with low inherent toxicity in the dark and efficient cell killing upon 980 nm irradiation. These findings support the continued investigation of designer isocorroles as promising agents for PTT. Compared to traditional PTAs, IC-PLGA NPs offer the advantage that they will not bioaccumulate like gold and are less susceptible to photobleaching than dye-based systems. Hence, the encapsulated isocorrole architectures are promising materials worthy of further study.

To expand upon this study, future work should examine the mechanism of cell death induced by IC-PLGA NPs upon irradiation, for example, by performing live/dead viability/cytotoxicity assays, evaluating cellular proliferation by EdU assay, or quantifying cellular apoptosis/necrosis by flow cytometry. These in-depth studies should be combined with *in vivo* work to explore the efficacy and safety of IC-PLGA NPs against TNBC in murine tumor models, as well as experiments to examine the potency of treatment against other forms of cancer since different cell types may have distinct responses to the NPs and thermal stress caused by PTT. For *in vivo* studies and clinical translation, the NPs would likely need to be modified to have a poly(ethylene glycol) or alternative “stealth” coating to maximize circulation time and tumor accumulation.

Expanding on the above points, future work should investigate both *in vitro* and *in vivo* the specific treatment parameters (e.g., IC-NP concentration, laser fluence, irradiation time) that yield apoptosis versus necrosis since the mechanism of cell death induced by PTT can impact the overall success of treatment.³⁶ For example, PTT-triggered immunogenic cell death provides a robust anti-tumor response that can synergize with immunotherapy approaches to enhance tumor eradication and prevent recurrence.⁴⁸ Forthcoming efforts from our labs will also explore strategies to further red-shift the absorption spectrum of the metalloisocorroles more fully into the NIR-II window. This will be important since wavelengths beyond 1000 nm penetrate tissue more effectively than the 980 nm light used in this work.

Overall, this work has pioneered the use of designer ICs as potent and safe mediators of PTT upon 980 nm excitation. With continued development to enhance their photophysical and biointerfacing properties, such materials may greatly advance the application of PTT near or within the NIR-II window.

ASSOCIATED CONTENT

Supporting Information

The Supporting Information is available free of charge at <https://pubs.acs.org/doi/10.1021/acsomega.2c04723>.

Methods for isocorrole synthesis; UV–visible absorption spectra of free and encapsulated isocorroles (Figure S1); NMR spectra of synthesized isocorroles (Figure S2–

S15); calculation of photothermal conversion efficiency (Figure S16); and crystallographic data and structure refinement details (Table S1) (PDF)

Accession Codes

CCDC 2206813–2206815 contain the supplementary crystallographic data for this paper. These data can be obtained free of charge via www.ccdc.cam.ac.uk/data_request/cif, or by emailing data_request@ccdc.cam.ac.uk, or by contacting the Cambridge Crystallographic Data Centre, 12 Union Road, Cambridge CB2 1EZ, UK; fax: +44 1223 336033.

AUTHOR INFORMATION

Corresponding Authors

Emily S. Day – Department of Biomedical Engineering and Department of Materials Science and Engineering, University of Delaware, Newark, Delaware 19716, United States; Helen F. Graham Cancer Center and Research Institute, University of Delaware, Newark, Delaware 19713, United States; orcid.org/0000-0002-8707-826X; Email: emilyday@udel.edu

Joel Rosenthal – Department of Chemistry and Biochemistry, University of Delaware, Newark, Delaware 19716, United States; orcid.org/0000-0002-6814-6503; Email: joelr@udel.edu

Authors

Maximilian R. J. Marek – Department of Biomedical Engineering, University of Delaware, Newark, Delaware 19716, United States

Trong-Nhan Pham – Department of Chemistry and Biochemistry, University of Delaware, Newark, Delaware 19716, United States; orcid.org/0000-0002-5087-0421

Jianxin Wang – Department of Biomedical Engineering, University of Delaware, Newark, Delaware 19716, United States; orcid.org/0000-0001-8621-543X

Quiqi Cai – Department of Chemistry and Biochemistry, University of Delaware, Newark, Delaware 19716, United States

Glenn P. A. Yap – Department of Chemistry and Biochemistry, University of Delaware, Newark, Delaware 19716, United States; orcid.org/0000-0003-0385-387X

Complete contact information is available at:

<https://pubs.acs.org/doi/10.1021/acsomega.2c04723>

Author Contributions

[†]M.J.R.M. and T.-N.P. contributed equally to this work. The manuscript was written through contributions of all authors. All authors have given approval to the final version of the manuscript.

Funding

This research was supported by the National Institute of General Medical Sciences (NIGMS) of the National Institutes of Health (NIH) under Award R35GM119659 (ESD) and by a grant from the Delaware Bioscience Center for Advanced Technology (J.R., E.S.D.). Portions of the isocorrole synthetic work were supported through the U.S. Department of Energy, Office of Science, Office of Basic Energy Sciences EPSCoR and Catalysis programs under Award Number DESC-0001234 (J.R.). Microscopy access was supported by grants from the NIH-NIGMS (P20-GM103446), the National Science Foundation (IIA-1301765), and the State of Delaware. X-ray

diffraction data collection was supported by the National Institutes of Health (S10-OD026896A).

Notes

The authors declare no competing financial interest.

ACKNOWLEDGMENTS

We thank Shannon Modla of the Delaware Bio-Imaging Center for assistance with transmission electron microscopy. GPAY wishes to thank M. I. Martin for X-ray diffraction data collection.

ABBREVIATIONS

PTT, photothermal therapy; NIR, near-infrared; TNBC, triple-negative breast cancer; PTA, photothermal agent; PLGA, poly(lactic-co-glycolic) acid; DPIC, diphenyl isocorrole

REFERENCES

- (1) Lu, Y.; Li, L.; Lin, Z.; Wang, L.; Lin, L.; Li, M.; Zhang, Y.; Yin, Q.; Li, Q.; Xia, H. A New Treatment Modality for Rheumatoid Arthritis: Combined Photothermal and Photodynamic Therapy Using Cu 7.2 S 4 Nanoparticles. *Adv. Healthcare Mater.* **2018**, *7*, No. 1800013.
- (2) Melamed, J. R.; Edelstein, R. S.; Day, E. S. Elucidating the Fundamental Mechanisms of Cell Death Triggered by Photothermal Therapy. *ACS Nano* **2015**, *9*, 6–11.
- (3) Riley, R. S.; O'Sullivan, R. K.; Potocny, A. M.; Rosenthal, J.; Day, E. S. Evaluating Nanoshells and a Potent Biladiene Photosensitizer for Dual Photothermal and Photodynamic Therapy of Triple Negative Breast Cancer Cells. *Nanomaterials* **2018**, *8*, No. 658.
- (4) Riley, R. S.; Day, E. S. Gold Nanoparticle-Mediated Photothermal Therapy: Applications and Opportunities for Multimodal Cancer Treatment. *WIREs Nanomed. Nanobiotechnol.* **2017**, *9*, No. e1449.
- (5) Wang, J.; Potocny, A. M.; Rosenthal, J.; Day, E. S. Gold Nanoshell-Linear Tetrapyrrole Conjugates for near Infrared-Activated Dual Photodynamic and Photothermal Therapies. *ACS Omega* **2020**, *5*, 926–940.
- (6) Bao, Z.; Liu, X.; Liu, Y.; Liu, H.; Zhao, K. Near-Infrared Light-Responsive Inorganic Nanomaterials for Photothermal Therapy. *Asian J. Pharm. Sci.* **2016**, *11*, 349–364.
- (7) Cao, J.; Zhu, B.; Zheng, K.; He, S.; Meng, L.; Song, J.; Yang, H. Recent Progress in NIR-II Contrast Agent for Biological Imaging. *Front. Bioeng. Biotechnol.* **2020**, *7*, No. 487.
- (8) Zhao, J.; Zhong, D.; Zhou, S. NIR-I-to-NIR-II Fluorescent Nanomaterials for Biomedical Imaging and Cancer Therapy. *J. Mater. Chem. B* **2018**, *6*, 349–365.
- (9) Sun, A.; Guo, H.; Gan, Q.; Yang, L.; Liu, Q.; Xi, L. Evaluation of Visible NIR-I and NIR-II Light Penetration for Photoacoustic Imaging in Rat Organs. *Opt. Express* **2020**, *28*, 9002–9013.
- (10) Jiang, Z.; Zhang, C.; Wang, X.; Yan, M.; Ling, Z.; Chen, Y.; Liu, Z. A Borondifluoride-Complex-Based Photothermal Agent with an 80% Photothermal Conversion Efficiency for Photothermal Therapy in the NIR-II Window. *Angew. Chem., Int. Ed.* **2021**, *60*, 22376–22384.
- (11) Wu, P.; Zhu, Y.; Chen, L.; Tian, Y.; Xiong, H. A Fast-Responsive OFF-ON Near-Infrared-II Fluorescent Probe for in Vivo Detection of Hypochlorous Acid in Rheumatoid Arthritis. *Anal. Chem.* **2021**, *93*, 13014–13021.
- (12) Duesterdieck-Zellmer, K. F.; Larson, M. K.; Plant, T. K.; Sundholm-Teppler, A.; Payton, M. E. Ex Vivo Penetration of Low-Level Laser Light through Equine Skin and Flexor Tendons. *Am. J. Vet. Res.* **2016**, *77*, 991–999.
- (13) Tortora, L.; Nardis, S.; Fronczek, F. R.; Smith, K. M.; Paolesse, R. Functionalization of the Corrole Ring: The Role of Isocorrole Intermediates. *Chem. Commun.* **2011**, *47*, 4243–4245.
- (14) Potocny, A. M.; Riley, R. S.; O'Sullivan, R. K.; Day, E. S.; Rosenthal, J. Photochemotherapeutic Properties of a Linear Tetrapyrrole Palladium(II) Complex Displaying an Exceptionally High Phototoxicity Index. *Inorg. Chem.* **2018**, *57*, 10608–10615.
- (15) Martin, M. I.; Cai, Q.; Yap, G. P. A.; Rosenthal, J. Synthesis, Redox, and Spectroscopic Properties of Pd(II) 10,10-Dimethylisocorrole Complexes Prepared via Bromination of Dimethylbiladiene Oligotetrapyrroles. *Inorg. Chem.* **2020**, *59*, 18241–18252.
- (16) Rice, A. T.; Martin, M. I.; Warndorf, M. C.; Yap, G. P. A.; Rosenthal, J. Synthesis, Spectroscopic, and 1O₂ Sensitization Characteristics of Extended Pd(II) 10,10-Dimethylbiladiene Complexes Bearing Alkynyl-Aryl Appendages. *Inorg. Chem.* **2021**, *60*, 11154–11163.
- (17) Cai, Q.; Rice, A. T.; Pointer, C. A.; Martin, M. I.; Davies, B.; Yu, A.; Ward, K.; Hertler, P. R.; Warndorf, M. C.; Yap, G. P. A.; Young, E. R.; Rosenthal, J. Synthesis, Electrochemistry, and Photophysics of Pd(II) Biladiene Complexes Bearing Varied Substituents at the Sp³-Hybridized 10-Position. *Inorg. Chem.* **2021**, *60*, 15797–15807.
- (18) Rice, A. T.; Yap, G. P. A.; Rosenthal, J. A P-61 Black Widow Inspired Palladium Biladiene Complex for Efficient Sensitization of Singlet Oxygen Using Visible Light. *Photochem* **2022**, *2*, 58–68.
- (19) Cai, Q.; Tran, L. K.; Qiu, T.; Eddy, J. W.; Pham, T.-N.; Yap, G. P. A.; Rosenthal, J. An Easily Prepared Monomeric Cobalt(II) Tetrapyrrole Complex That Efficiently Promotes the 4e⁻/4H⁺ Peractivation of O₂ to Water. *Inorg. Chem.* **2022**, *61*, 5442–5451.
- (20) Larsen, S.; McCormick, L. J.; Ghosh, A. Rapid One-Pot Synthesis of Pyrrole-Appended Isocorroles. *Org. Biomol. Chem.* **2019**, *17*, 3159–3166.
- (21) Costa, R.; Geier, G. R., III; Ziegler, C. J. Structure and Spectroscopic Characterization of Free Base and Metal Complexes of 5,5-Dimethyl-10,15-Bis(Pentafluorophenyl)Isocorrole. *Dalton Trans.* **2011**, *40*, 4384–4386.
- (22) Pomarico, G.; Xiao, X.; Nardis, S.; Paolesse, R.; Fronczek, F. R.; Smith, K. M.; Fang, Y.; Ou, Z.; Kadish, K. M. Synthesis and Characterization of Free-Base, Copper, and Nickel Isocorroles. *Inorg. Chem.* **2010**, *49*, 5766–5774.
- (23) Foroutan-Nejad, C.; Larsen, S.; Conradie, J.; Ghosh, A. Isocorroles as Homoaromatic NIR-Absorbing Chromophores: A First Quantum Chemical Study. *Sci. Rep.* **2018**, *8*, No. 11952.
- (24) Isakoff, S. J. Triple Negative Breast Cancer: Role of Specific Chemotherapy Agents. *Cancer J.* **2010**, *16*, 53–61.
- (25) Wahba, H. A.; El-Hadaad, H. A. Current Approaches in Treatment of Triple-Negative Breast Cancer. *Cancer Biol. Med.* **2015**, *12*, 106–116.
- (26) Lee, J. H.; Kim, S. H.; Suh, Y. J.; Shim, B. Y.; Kim, H. K. Predictors of Axillary Lymph Node Metastases (ALNM) in a Korean Population with T1-2 Breast Carcinoma: Triple Negative Breast Cancer Has a High Incidence of ALNM Irrespective of the Tumor Size. *Cancer Res. Treat.* **2010**, *42*, No. 30.
- (27) Anders, C. K.; Carey, L. A. Biology, Metastatic Patterns, and Treatment of Patients with Triple-Negative Breast Cancer. *Clin. Breast Cancer* **2009**, *9*, S73–S81.
- (28) Uhm, J. E.; Park, Y. H.; Yi, S. Y.; Cho, E. Y.; Choi, Y. L.; Lee, S. J.; Park, M. J.; Lee, S. H.; Jun, H. J.; Ahn, J. S.; Kang, W. K.; Park, K.; Im, Y. H. Treatment Outcomes and Clinicopathologic Characteristics of Triple-Negative Breast Cancer Patients Who Received Platinum-Containing Chemotherapy. *Int. J. Cancer* **2009**, *124*, 1457–1462.
- (29) Zhang, L.; Liu, C.; Gao, Y.; Li, Z.; Xing, J.; Ren, W.; Zhang, L.; Li, A.; Lu, G.; Wu, A.; Zeng, L. ZD2-Engineered Gold Nanostar@Metal-Organic Framework Nanoprobes for T1-Weighted Magnetic Resonance Imaging and Photothermal Therapy Specifically Toward Triple-Negative Breast Cancer. *Adv. Healthcare Mater.* **2018**, *7*, No. 1801144.
- (30) Zhang, M.; Kim, H. S.; Jin, T.; Moon, W. K. Near-Infrared Photothermal Therapy Using EGFR-Targeted Gold Nanoparticles Increases Autophagic Cell Death in Breast Cancer. *J. Photochem. Photobiol. B* **2017**, *170*, 58–64.
- (31) Chen, G.; Ma, B.; Wang, Y.; Xie, R.; Li, C.; Dou, K.; Gong, S. CuS-Based Theranostic Micelles for NIR-Controlled Combination

Chemotherapy and Photothermal Therapy and Photoacoustic Imaging. *ACS Appl. Mater. Interfaces* **2017**, *9*, 41700–41711.

- (32) Apex3; Bruker AXS Inc.: Madison, WI, 2015.
- (33) Sheldrick, G. M. SHELXT - Integrated Space-Group and Crystal-Structure Determination. *Acta Crystallogr., Sect. A: Found. Adv.* **2015**, *71*, 3–8.
- (34) Sheldrick, G. M. Crystal Structure Refinement with SHELXL. *Acta Crystallogr., Sect. C: Struct. Chem.* **2015**, *71*, 3–8.
- (35) Spek, A. L. PLATON SQUEEZE: A Tool for the Calculation of the Disordered Solvent Contribution to the Calculated Structure Factors. *Acta Crystallogr., Sect. C: Struct. Chem.* **2015**, *71*, 9–18.
- (36) Valcourt, D. M.; Dang, M. N.; Day, E. S. IR820-Loaded PLGA Nanoparticles for Photothermal Therapy of Triple-Negative Breast Cancer. *J. Biomed. Mater. Res., Part A* **2019**, *107*, 1702–1712.
- (37) Mori, H.; Naoda, K.; Osuka, A. Bottom-Up Synthesis of Bis(Triisopropylsilyl)Ethyne Hexaphyrin Bearing an Unsubstituted Meso-Carbon. *Asian J. Org. Chem.* **2013**, *2*, 600–605.
- (38) Gowri Sreedevi, K.; Thomas, A. P.; Salini, P. S.; Ramakrishnan, S.; Anju, K. S.; Holaday, M. G. D.; Reddy, M. L. P.; Suresh, C. H.; Srinivasan, A. 5,5-Diaryldipyrromethanes: Syntheses and Anion Binding Properties. *Tetrahedron Lett.* **2011**, *52*, S995–S999.
- (39) Rao, P. D.; Littler, B. J.; Geier, G. R.; Lindsey, J. S. Efficient Synthesis of Monoacyl Dipyrromethanes and Their Use in the Preparation of Sterically Unhindered Trans-Porphyrins. *J. Org. Chem.* **2000**, *65*, 1084–1092.
- (40) Flint, D. L.; Fowler, R. L.; LeSaulnier, T. D.; Long, A. C.; O'Brien, A. Y.; Geier, G. R. Investigation of Complementary Reactions of a Dipyrromethane with a Dipyrromethanemonocarbonyl Leading to a 5-Isocorrole. *J. Org. Chem.* **2010**, *75*, 553–563.
- (41) Gouterman, M.; Wagnière, G. H.; Snyder, L. C. Spectra of Porphyrins: Part II. Four Orbital Model. *J. Mol. Spectrosc.* **1963**, *11*, 108–127.
- (42) Thomas, K. E.; Beavers, C. M.; Gagnon, K. J.; Ghosh, A. β -Octabromo- and β -Octakis(Trifluoromethyl)Isocorroles: New Sterically Constrained Macrocyclic Ligands. *ChemistryOpen* **2017**, *6*, 402–409.
- (43) Maeda, H.; Wu, J.; Sawa, T.; Matsumura, Y.; Hori, K. Tumor Vascular Permeability and the EPR Effect in Macromolecular Therapeutics: A Review. *J. Controlled Release* **2000**, *65*, 271–284.
- (44) Sindhwani, S.; Syed, A. M.; Ngai, J.; Kingston, B. R.; Maiorino, L.; Rothschild, J.; MacMillan, P.; Zhang, Y.; Rajesh, N. U.; Hoang, T.; Wu, J. L. Y.; Wilhelm, S.; Zilman, A.; Gadde, S.; Sulaiman, A.; Ouyang, B.; Lin, Z.; Wang, L.; Egeblad, M.; Chan, W. C. W. The Entry of Nanoparticles into Solid Tumours. *Nat. Mater.* **2020**, *19*, 566–575.
- (45) Alexis, F.; Pridgen, E.; Molnar, L. K.; Farokhzad, O. C. Factors Affecting the Clearance and Biodistribution of Polymeric Nanoparticles. *Mol. Pharmaceutics* **2008**, *5*, 505–515.
- (46) Roper, D. K.; Ahn, W.; Hoepfner, M. Microscale Heat Transfer Transduced by Surface Plasmon Resonant Gold Nanoparticles. *J. Phys. Chem. C* **2007**, *111*, 3636–3641.
- (47) Xu, D.; Liu, J.; Wang, Y.; Jian, Y.; Wu, W.; Lv, R. Black Phosphorus Nanosheet with High Thermal Conversion Efficiency for Photodynamic/Photothermal/Immunotherapy. *ACS Biomater. Sci. Eng.* **2020**, *6*, 4940–4948.
- (48) Chen, Y.; Guo, Y.; Han, P.; Li, D.; Gui, X.; Zhang, Z.; Fu, K.; Chu, M. Graphitic Carbon Nanocages as New Photothermal Agent and Drug Carrier for 980-Nm-Laser-Driven Cancer Therapy. *Carbon* **2018**, *136*, 234–247.
- (49) Bi, C.; Chen, J.; Chen, Y.; Song, Y.; Li, A.; Li, S.; Mao, Z.; Gao, C.; Wang, D.; Möhwald, H.; Xia, H. Realizing a Record Photothermal Conversion Efficiency of Spiky Gold Nanoparticles in the Second Near-Infrared Window by Structure-Based Rational Design. *Chem. Mater.* **2018**, *30*, 2709–2718.
- (50) Dang, M. N.; Casas, C. G.; Day, E. S. Photoresponsive MiR-34a/Nanoshell Conjugates Enable Light-Triggered Gene Regulation to Impair the Function of Triple-Negative Breast Cancer Cells. *Nano Lett.* **2021**, *21*, 68–76.

(51) Kim, S.; Lee, S. Y.; Cho, H. J. Berberine and Zinc Oxide-Based Nanoparticles for the Chemo-Photothermal Therapy of Lung Adenocarcinoma. *Biochem. Biophys. Res. Commun.* **2018**, *501*, 765–770.

(52) Namvar, F.; Rahman, H. S.; Mohamad, R.; Azizi, S.; Tahir, P. M.; Chartrand, M. S.; Yeap, S. K. Cytotoxic Effects of Biosynthesized Zinc Oxide Nanoparticles on Murine Cell Lines. *Evidence-Based Complementary Altern. Med.* **2015**, *2015*, No. 593014.

Recommended by ACS

Conjugated Polymer Coupled with Nonconjugated Segments for NIR-II Fluorescence/NIR-II Photoacoustic Imaging-Guided NIR-II Photothermal Therapy

Danni Hu, Quli Fan, *et al.*

SEPTEMBER 25, 2023

ACS APPLIED POLYMER MATERIALS

READ 

A Novel Hexokinases Inhibitor Based on Molecularly Imprinted Polymer for Combined Starvation and Enhanced Photothermal Therapy of Malignant Tumors

Ji Zhuang, Yu-Kui Zhang, *et al.*

MAY 16, 2023

ACS APPLIED MATERIALS & INTERFACES

READ 

Terminalia chebula Polyphenol and Near-Infrared Dye-Loaded Poly(lactic acid) Nanoparticles for Imaging and Photothermal Therapy of Cancer Cells

Monika Pebam, Aravind Kumar Rengan, *et al.*

OCTOBER 26, 2022

ACS APPLIED BIO MATERIALS

READ 

Smart Chemical Oxidative Polymerization Strategy To Construct Au@PPy Core-Shell Nanoparticles for Cancer Diagnosis and Imaging-Guided Photothermal Therapy

Chunxiao Sui, Wengui Xu, *et al.*

DECEMBER 14, 2022

BIOCONJUGATE CHEMISTRY

READ 

Get More Suggestions >